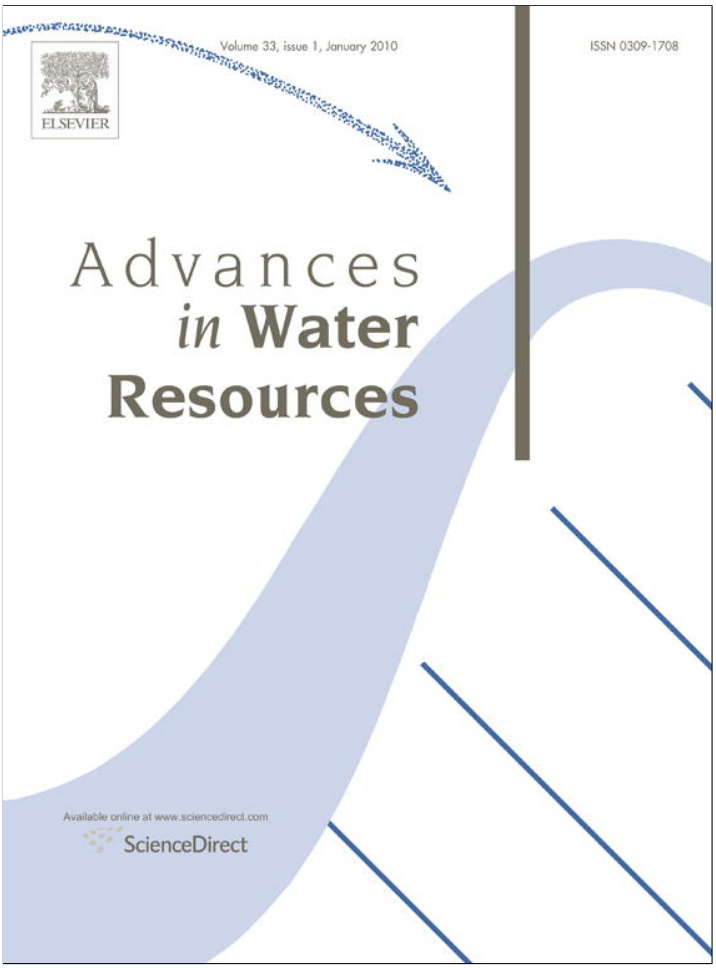

Advances in Water Resources 33 (2010) 106–122

Contents lists available at ScienceDirect

Advances in Water Resources

journal homepage: www.elsevier.com/locate/advwatres

Development and testing of a physically based, three-dimensional model of surface and subsurface hydrology

Marco Bittelli [a,*], Fausto Tomei [b], Alberto Pistocchi [c], Markus Flury [d], Jan Boll [e], Erin S. Brooks [e], Gabriele Antolini [b]

[a] Department of AgroEnvironmental Science and Technology, University of Bologna, Italy
[b] Environmental Protection Agency of Emilia-Romagna, HydroMeteoClimate Service (ARPA-SIMC), Bologna, Italy
[c] Institute for Environment and Sustainability (IES), European Community Joint Research Center, Ispra, Italy
[d] Department of Crop and Soil Sciences, Washington State University, Pullman, WA, USA
[e] Department of Biological and Agricultural Engineering, University of Idaho, Moscow, ID, USA

ARTICLE INFO

Article history:
Received 2 April 2009
Received in revised form 21 October 2009
Accepted 26 October 2009
Available online 30 October 2009

Keywords:
Surface hydrology
Subsurface hydrology
Models
Physically based
Catchment
Distributed

ABSTRACT

We present a numerical, catchment-scale model that solves flow equations of surface and subsurface flow in a three-dimensional domain. Surface flow is described by the two-dimensional parabolic approximation of the St. Venant equation, using Manning's equation of motion; subsurface flow is described by the three-dimensional Richards' equation for the unsaturated zone and by three-dimensional Darcy's law for the saturated zone, using an integrated finite difference formulation. The hydrological component is a dynamic link library implemented within a comprehensive model which simulates surface energy, radiation budget, snow melt, potential evapotranspiration, plant development and plant water uptake. We tested the model by comparing distributed and integrated three-dimensional simulated and observed perched water depth (PWD), stream flow data, and soil water contents for a small catchment. Additional tests were performed for the snow melting algorithm as well as the different hydrological processes involved. The model successfully described the water balance and its components as evidenced by good agreement between measured and modelled data.

1. Introduction

In recent decades, important advances have been made in the development of catchment-scale hydrological models for practical applications and decision support [12]. The increase of computing power and availability of hydrological data at different scales, has enhanced the availability and testing of hydrological models. The use of hydrological models for predictive or management purposes, however, depends on the quality of model parameters and model calibration [11].

Mathematical description of the hydrological system can follow the physical, the conceptual, or the systems approach [12], depending on the purpose of model development and application. Models based on the physical approach (also referred to as physically based models) typically are based on the solution of general conservation equations of fluid mechanics with appropriate boundary conditions [1]. One of the advantages of implementing physically based models is that physical constraints can be used to reduce the range of model parameters [37]. This is particularly helpful in the case of distributed models, where the same output can be obtained by multiple combinations of state parameters (such as soil moisture), often making the model ill-defined [6] and stressing the importance of soil moisture measurements as a very important variable for model testing [61]. Physically based models provide a consistent way of estimating soil moisture distribution, runoff generation patterns, and stream flow [56,11].

Grayson and Blöschl [26] made the case for the dominant process concept, proposing to develop methods to identify dominant processes that control hydrological response, and developing models to focus on these dominant processes. Sivakumar [50], while embracing the dominant processes concept, suggested that simplification is the key for an effective way to model hydrological systems. Clearly, to evaluate the simplification process, a rigorous modelling approach must be used as a benchmark, along with appropriate observations.

Having a single model that describes the entire water cycle with appropriate equations of flow involves a large computational burden and numerical complexities when coupling domains with different characteristic time scales. In selecting a benchmark model,

* Corresponding author. Tel.: +39 051 2096695; fax: +39 051 2096241.
E-mail address: marco.bittelli@unibo.it (M. Bittelli).

0309-1708/$ - see front matter © 2009 Elsevier Ltd. All rights reserved.
doi:10.1016/j.advwatres.2009.10.013

we examined the literature for physically based hydrological models and we divided the models in three categories based on: (1) dimensional simplification; (2) domain simplification; and (3) replacement of physical equations with simplified, semi-empirical models.

In the first category, the SHE (Système Hydrologique Européen) model, is a comprehensive physically based model [5], describing two-dimensional surface and groundwater flow coupled through a one-dimensional solution of Richards' equation. The model has been subsequently enhanced by introducing additional hydrological processes such as solute and sediment transport. The SHE model, however, does not simulate subsurface lateral flow, an important driver of water and material transport in many landscapes. A similar comprehensive physically based, distributed model is DHSVM (Distributed Hydrology Soil Vegetation Model), which includes subsurface lateral flow [60]. Recently, DHSVM was enhanced to simulate soil erosion and sediment transport [18].

In the second category, simplified domain models are the ones describing one part of the hydrological cycle explicitly, such as groundwater flow (with or without the vadose zone): e.g., CODESA3D [23], SUTRA [59], MODFLOW [29], channel and overland flow [25,16], hillslope hydrology (e.g., Hsb [53]), subsurface hydrological flow processes [47,55] and MACRO [33]. A more comprehensive model (including heat and solute transport) that utilized simplified domains for saturated/unsaturated flow in the vadose zone is HYDRUS-2D/3D [54]. In these cases, the physical flow and transport equations are solved rigorously, but only with reference to a simplified spatial domain, while simplifying or omitting processes, such as surface–groundwater interactions or surface runoff.

In the third category, models include many processes currently considered relevant for the water balance, soil erosion and/or contaminant transport, but the physical equations are simplified. Examples include TOPMODEL [7], the Generalized Loading Function (GWLF) [28], THALES [27], Soil and Water Assessment Tool (SWAT) [4], the Water Erosion Prediction Project (WEPP) [21], and the Soil Moisture Routing (SMR) model [22,11] also referred to as the Soil Moisture Distribution Routing (SMDR) [24]. These models are applicable within the limits in which the methods implemented are validated, and cannot be considered as fully physically based.

The choice of a model is sometimes dependent on the data available, but at the same time the planning of data acquisition campaigns is increasingly related to the model structure chosen, so that it appears advisable to provide methods to judge simplified models *a priori*, by comparing their answer to given inputs with the corresponding answer that a "non-simplified," state-of-the-art model would provide. This is particularly important in local, detailed modelling where conceptual models fail to predict detailed aspects of the phenomena involved, and when simplifications in conceptual models are such that benchmarking with a more comprehensive model are sought (e.g. [14,56,37]).

In this paper, we present a physically based, three-dimensional catchment-scale model applicable to small catchments. Based on the previous classification, our model is a physically based hydrological model coupled with conceptual models for snow accumulation and melting, soil evaporation and plant transpiration. The model has the following features: (a) an algorithm for coupling the surface and the surface flow components with simultaneous solution of one conservation equation, (b) it is not calibrated, and (c) it is comprehensive of various modules which make it applicable in many different topographical and environmental conditions.

We verified the model using distributed and integrated response data from the a catchment in Troy, Idaho. Our hydrological model includes both saturated and unsaturated subsurface flow, as well as overland flow, soil evaporation, snow accumulation and melt and plant water uptake. The model uses digital terrain model (DTM) data as a basic structure for the grid generation used for the computational nodes, and it is equipped with an user windows interface that allows model input, model output, parameter setting and 3D visualization of many properties of interest. Our model is intended to simulate three-dimensional hydrological patterns in small catchments, especially when phenomena related to surface runoff coupled with subsurface flow are of interest, and it can be used as a benchmark model.

2. Model description

2.1. General description

The model, named Criteria-3D, is based on the integrated finite difference (also called cell-centered finite volume scheme) method [15]. The model accounts for saturated water flow, unsaturated water flow and surface runoff, and it is coupled with conceptual models for soil evaporation, snow accumulation and melt, plant water uptake, and topography-dependent solar radiation. Spatial information needed for the hydrological model is provided by a DTM, a soil map with parameters for hydraulic properties and a land use map with the Manning's parameters. Criteria-3D needs hourly sink–source data (precipitation, snow melt, soil evaporation, plant water uptake), which are generated by the conceptual models included in the software that require hourly data of precipitation, temperature, relative humidity, wind velocity and solar radiation. Moreover, land use maps and crop parameters are needed.

Soil mapping units are represented by reference soil profiles with specific hydraulic properties for individual soil layers. The model allows for including both horizontal and vertical soil variability. It is therefore possible to use spatially distributed soil profiles, with different horizon depths and total depths of the profile.

The model allows coupling with raster data sets from GIS, although it is equipped with an interface for 3D visualization, and data management. All soil and topographic information are provided as Arcview Binary Raster format (.flt). The spatially resolved results (soil moisture, hydraulic heads, flow fields) are also produced as Binary Raster format (.flt) or ASCII grid format readable by most GIS packages.

A catchment is simulated as an integrated three-dimensional system, and the whole hydrologically active geometry (i.e., the surface and subsoil down to an impervious layer) should be provided as input to the model. The boundary condition at the catchment bottom is either a no flow or a free drainage condition.

Atmospheric boundary conditions are either positive flux (precipitation) assigned to the surface, or negative flux (potential evapotranspiration) to the upper soil layer and rooting depth, respectively. Potential evaporation and transpiration are limited to their actual values by actual soil water availability. The model does not simulate preferential flow, solute transport, and channel flow. Preferential flow can be emulated by using "effective" soil properties (e.g., increased porosity and hydraulic conductivity), if such data are available. Channel flow plays an increasingly important role as the stream network becomes more and more complex. However, for small catchments it can be argued that the modification of hydrographs occurring in the stream network is less important than the formation of the hydrograph from overland and lateral subsurface flow.

2.2. Governing equations

$$\frac{\partial(W\theta)}{\partial t} = -\mathrm{div}(u) + q \tag{1}$$

where u is the flux, W is the total available volume at a node, θ is the volumetric water content and q is the water input or output (expressed as a volume). This general equation is solved adopting two different laws to describe fluxes within the soil matrix and fluxes on the soil surface. In the first case, we employ the Richards' equation:

$$W\frac{d\theta}{dH}\frac{\partial H}{\partial t} = \mathrm{div}[K(h)\cdot \mathrm{grad}(H)] + q \tag{2}$$

$K(h)$ is the hydraulic conductivity and H is the total hydraulic head. The total hydraulic head (H) is given by the sum of elevation z (or gravitational component) and the hydraulic matric component $h = p/g\rho_w$, where ρ_w is the water density, p the soil matric potential, g is the gravitational acceleration and t is time. For saturated flow, Eq. (2) reduces to the Laplace equation for groundwater flow, under the assumption of steady flow, homogeneity and isotropy of hydraulic properties.

For surface flow, the volume upon which the mass balance is computed varies according to the surface hydraulic depth, h_s, which results in a surface storage term $W = Sh_s$, where S is the planimetric surface area. These assumption allows to rewrite the second term in Eq. (1) as:

$$\frac{\partial(W\theta)}{\partial t} = S\frac{\partial h_s}{\partial t} = S\frac{\partial H}{\partial t} \tag{3}$$

Assuming the depth h_s is much smaller than the flow width, the velocity along the coordinate x is given by Manning's equation adopting h_s as the hydraulic radius:

$$u_x = -\left(\frac{h_s^{0.67}}{M}\right)\sqrt{\frac{\partial H}{\partial x}} \tag{4}$$

where M is the Manning's roughness coefficient. In two dimensions, Manning's equation can be written as [16]:

$$u_m = -K^*(H, h_s)\mathrm{grad}\,H \tag{5}$$

where K^* is a conveyance function depending on H and h_s according to:

$$K^* = \frac{\left(\frac{h_s^{0.67}}{M}\right)}{\sqrt[4]{\left(\frac{\partial H}{\partial x}\right)^2 + \left(\frac{\partial H}{\partial y}\right)^2}} \tag{6}$$

Substitution of Eqs. (3) and (5) into Eq. (1) yields:

$$S\frac{\partial H}{\partial t} = \mathrm{div}[K^*(H, h_s)\cdot \mathrm{grad}(H)] + q \tag{7}$$

which is the well-known parabolic (or "diffusion wave") approximation of the St. Venant equation.

The Richards' equation for flow in variably saturated soil and the parabolic St. Venant equation for surface flow have equivalent mathematical structure that can be expressed in the unified form:

$$C\frac{\partial H}{\partial t} = \mathrm{div}[K'\cdot \mathrm{grad}(H)] + q \tag{8}$$

where

$$C = \begin{cases} S & \text{for Surface flow} \\ W\frac{d\theta}{dH} & \text{for Subsurface flow} \end{cases} \tag{9}$$

and

$$K' = \begin{cases} K^* & \text{for Surface flow} \\ K & \text{for Subsurface flow} \end{cases} \tag{10}$$

The surface flow depth is considered as the total depth of water on the surface minus the inactive water depth which is retained in microtopography (tillage, different cropping systems).

Overall, the mathematical and numerical formulation of the continuity equation (as expressed in the Richards' and St. Venant equations) is the basis for the coupling of the surface and subsurface components. This scheme allows to simultaneously solve both equations (surface and subsurface) by deriving one mass balance equation only, for both surface and subsurface flow. For the subsurface flow the element volumes are constant and the volumetric water content changes (Richards' equation) while in the surface flow the element volumes may change (depending on precipitation, and fluxes in and out from other surface nodes) while the water content of the node is always at saturation ($\theta = 1$). The term W in the continuity equation allows for changing in the total volume of the computational node for the surface nodes. In Appendix A, a detailed description of the coupling between surface and subsurface is provided.

2.3. Soil hydraulic properties

The soil water retention data are described by the van Genuchten equation [58]

$$\theta(h) = \theta_r + (\theta_s - \theta_r)\left(\frac{1}{[1 + (\alpha h)^n]^m}\right) \tag{11}$$

where $\theta(h)$ is the volumetric water content at the water potential h, θ_s and θ_r are the saturated and residual water contents, respectively, α is the coordinate of the inflexion point of the retention curve, and n is a dimensionless factor related to the pore-size distribution. We used the restriction $m = 1 - 1/n$.

The hydraulic conductivity was calculated by the model of Mualem [41]

$$K(h) = \frac{K_s(1 - (\alpha h)^{mn}[1 + (\alpha h)^n]^{-m})^2}{[1 + (\alpha h)^n]^{ml}} \tag{12}$$

where K_s is the saturated hydraulic conductivity, and l is an empirical parameter that accounts for pore tortuosity. We used $l = 0.5$.

Ippisch et al. [31] pointed out that the van Genuchten–Mualem model, under certain conditions, is problematic when water retention data are used to predict the hydraulic conductivities and they demonstrated that if $n < 2$ or $\alpha h_a > 1$ (where h_a is the air-entry value of the soil, corresponding to the largest pore radius), the van Genuchten–Mualem model predicts erroneous hydraulic conductivities. In these cases, an explicit air-entry value, h_e, has to be included, leading to a modified van Genuchten–Mualem model [31]:

$$S_e = \begin{cases} \frac{1}{S_c}[1 + (\alpha h)^n]^{-m} & \text{if } (h \leqslant h_e) \\ 1 & \text{if } (h > h_e) \end{cases} \tag{13}$$

where S_e is the degree of saturation, α, m, n are fitting parameters, and $S_c = [1 + (\alpha h_e)^n]^{-m}$ is the water saturation at the air-entry potential h_e (the water potential is expressed as a negative number). The resulting hydraulic conductivity using the Mualem model is:

$$K = \begin{cases} K_s S_e^l\left[\frac{1-(1-(S_e S_c)^{1/m})^m}{1-(1-S_c^{1/m})^m}\right]^2 & \text{if } (S_e < 1) \\ K_s & \text{if } (S_e \geqslant 1) \end{cases} \tag{14}$$

where l is the same parameter as in the original Mualem equation. Ippisch et al. [31] suggested that h_e can be obtained either from knowledge of the largest pore size or by inverse modelling. In this study we implemented both the original van Genuchten–Mualem model (to be used for n values larger than 2) and the modified van Genuchten–Mualem model if the water retention fitting yields n values smaller than 2. The user can choose from these two options from the user window interface. Moreover, the software is equipped with a non-linear fitting algorithm [39] that allow to fit the hydrau-

lic property models, by inputting experimental data for the soil water retention.

Since the van Genuchten parameters obtained from the experimentally determined soil water retention provided $n < 2$, the simulations for the Troy catchment were performed using the modified van Genuchten–Mualem model.

2.4. Boundary conditions

The model allows to specify time and space-dependent boundary conditions: (1) nodes with fixed hydraulic head, (2) nodes set at atmospheric boundary conditions, (3) nodes with prescribed flux, and (4) nodes with no flux. The model allows to set small subsurface discretization nodes, to assure accurate resolution of surface–subsurface coupling. The computational structure allows describing the aquifer base or bedrock (bottom boundary of the computational domain) of irregular shapes and various depths.

In this model a constant hydraulic head corresponding to saturated condition was used, as a boundary condition at the outlet. In many situations when simulating a catchment, it is assumed that water always exits the catchment at an outlet. This assumption corresponds reasonably well to catchment outlets not affected by strongly varying water levels downstream, as in most small catchments entirely drained by the stream network downstream. When such situation is met, it is desirable to have a constant head condition at the outlet sufficiently low to ensure drainage from the catchment. It is reasonable to assume that the catchment outlet be the closest to saturated conditions, as predicted by TOPMODEL [7] or the model proposed by Svetlitchnyi et al. [51].

2.5. Solar radiation

Surface radiation is needed to compute snow melt and evapotranspiration. Clear-sky short wave radiation is computed using the algorithms implemented in *r.sun*, an open source code included in the GIS software GRASS [30,43]. Latitude, elevation, slope and aspect (which can be computed from elevation taken from a DTM) and local solar time are the input data for computing sun position, in terms of azimuth and elevation. Shadowing due to relief is taken into account by using a DTM. Clear-sky short wave hourly irradiance is obtained as the summation of beam, diffuse and reflected components. Attenuation by clear-sky atmosphere and consequently beam and diffuse components are modelled by the Linke [35] turbidity factor. Reflected irradiance is computed using an albedo coefficient. Real-sky (i.e., overcast) hourly irradiance for a horizontal surface is estimated using global transmissivity, computed as the ratio between clear-sky irradiance and actual irradiance maps. These are obtained by spatial interpolation of hourly global irradiance station data. However, for inclined surfaces, separation between beam and diffuse transmissivities is needed, if beam and diffuse irradiance data are not available separately. For this purpose, we adapted the equation proposed by Bristow and Campbell [8] to be used also with hourly irradiance data. The topography-dependent solar radiation was used for both the snow accumulation and melt algorithm as well as for soil evapotranspiration.

2.6. Snow melt

Snow melt is based on the algorithm presented by Brooks [9] and Brooks et al. [11]. The algorithm is based on the computation of mass and energy balance of the snow pack. Snow drifts are computed based on the model Snow Tran-3D model [36], and adjusted based on hourly measurements of wind speed. We improved the original snow melting model by Brooks [9] by including the effect of stream flow kinetic energy on snow melt. The energy associated with runoff per unit area or stream power for sheet flow, (Ω_s, W m^{-2}), was determined from

$$\Omega_s = \rho_w g S q_w \tag{15}$$

where ρ_w is the density of water, g is the gravitational acceleration, S is the sine of the erosion surface slope, and q_w is the volumetric runoff per unit width of erosion surface [48]. The effect of runoff liquid water temperature on snow melting was also included, by using a similar approach to the one by Brooks [9], where the advective heat transfer driven by the temperature gradient between rainfall water and the snow pack, was included in the snow energy budget. We also included the advective exchange between runoff water and the snow pack.

2.7. Evaporation and transpiration

Potential evapotranspiration *ETP* is calculated by Penman-Monteith [2] for the typical reference crop. The potential evapotranspiration for the actual crop (ET_0) is computed by:

$$ET_0 = ETP \times Kc \tag{16}$$

where the crop coefficient (Kc) is obtained by:

$$Kc = Kc_{ref} \times TC \tag{17}$$

where Kc_{ref} is a function of the leaf area index (LAI):

$$Kc_{ref} = 1 - (0.67e^{(-0.8LAI)}) \tag{18}$$

while TC is a turbulence coefficient determined by [38]:

$$TC = 1 + \frac{(TC_{max} - 1)(Kc_{ref} - 0.33)}{0.67} \tag{19}$$

where TC_{max} is the maximum of TC, dependent on the crop and coinciding with the maximum value of the crop coefficient Kc [17].

The algorithm for plant transpiration is based on the approach of Driessen and Konijn [20], where maximum transpiration (T_0) is computed from the potential evapotranspiration (ETP):

$$T_0 = ETP \times TC \frac{(Kc_{ref} - 0.33)}{0.67} \tag{20}$$

and the maximum soil evaporation (E_0) is computed by:

$$E_0 = ET_0 - T_0 \tag{21}$$

Actual soil evaporation is limited by soil water content with a quasi-linearly decreasing function depending on soil depth in the first superficial layers (usually 20 cm). Actual transpiration (T) is obtained by reducing the maximum transpiration (T_0) depending on soil water potential and root density. The soil layers that contribute to transpiration are determined by root depth [20]. The model allows selecting among several root shapes, depths and density, based on several crop types.

3. Numerical formulation

The solution of the governing equations is based on the integrated finite difference method which consists in the integration of the differential continuity equation over a finite domain D, as described in de Marsily [15], leading to the integral equation:

$$\iiint \mathrm{div}(u)\,dx\,dy\,dz + \iiint \frac{\partial(W\theta)}{\partial t}\,dx\,dy\,dz = \iiint q\,dx\,dy\,dz \tag{22}$$

The mass balance is computed for the spatial unit D of the model domain. Based on integral properties, Eq. (22) can be written as:

$$\int_{\Gamma_D} u \cdot n^*\,dS + \iiint \frac{\partial(W\theta)}{\partial t}\,dx\,dy\,dz = \iiint q\,dx\,dy\,dz \tag{23}$$

where Γ_D is the surface of the computational domain D, and n^* its normal unit vector. Eq. (22) can be applied over a simulation volume within which the material properties are constant.

If the simulation domain is approximated by a three-dimensional grid of nodes, Eq. (23) is equivalent to the mass balance equation for the volume surrounding each node:

$$\frac{\partial V_i}{\partial t} = \sum_{j=1}^{n} Q_{ij} + q_i \quad \forall i \neq j \tag{24}$$

where V_i is the amount of stored water in the volume surrounding the node, Q_{ij} is the flux between the ith and the jth node, and q_i is the input flux at the ith node. We can write a system of equations for all nodes with the unknowns being the hydraulic potentials, H.

The flux Q_{ij} is described by Darcy's law in finite difference form:

$$Q_{ij} = -K_{ij} S_{ij} \frac{(H_i - H_j)}{L_{ij}} \tag{25}$$

where S_{ij} is the interfacial area between nodes i and j, L_{ij} is the distance between the two nodes, H_i is the hydraulic potential at node i, and K_{ij} is the internode conductivity. The model allow the user to choose the geometric mean of nodal conductivities $K_{ij} = \sqrt{(K_i K_j)}$, where K_i is the hydraulic conductivity at the ith node, or the harmonic mean $K_{ij} = 2/(1/K_i + 1/K_j)$. The user can choose from these two options from the window user interface. In this study the harmonic mean was choose. For calculating the exchanges between surface and the first soil layer, the soil conductivity is based on the degree of water saturation. For surface flow, the only required parameters are Manning's roughness and the depth of the ponding layer. The details of the numerical implementation are given in Appendix A.

3.1. Convergence and mass balance errors

The convergence of the iteration can be checked by employing the infinite norm [44]:

$$\|H^{(k)} - H^{(k-1)}\|_{\inf} = \max_{i=1,\ldots,n} |H^{(k)} - H^{(k-1)}| \tag{26}$$

where H are the unknown water potentials. Convergence is reached if the norm is less than 10^{-14} [m], and the number of iterations for every approximation is <100. However, the reduction of the defect based on a sufficient reduction of the initial defect is limited because there is no unique defect formulation for non-linear system, and the reduction of the error based on the change in the target variable does not necessarily provide a good convergence.

A better convergence algorithm is the defect-correction method. The defect-correction method [49] is an iterative method that allow to increase the accuracy of a computed solution without the need for grid refinement. In general, the basic technique can be simply described as follows. The residual or defect is find first, and used to solve for the error or correction either via the non-linear update or the linear update, in order to obtain the corrected solution [32].

As suggested by Morton and Mayers [40], we used the mass balance ratio:

$$MBR = \frac{\Delta storage}{flux_{in} - flux_{out}} \tag{27}$$

to evaluate the precision in computing the mass conservation equation. Here *storage* is the amount of water stored in the computing element at time t, and $flux_{in}$ and $flux_{out}$ are the fluxes into and out of the element. In a fully mass conservative system *MBR* should be equal to 1. When the fluxes are very small, Eq. (27) can generate numeric overflow because of division by zero [52], and therefore we modified the *MBR*:

$$MBR_m = \frac{storage_{t+\Delta t}}{storage_t + flux_{in} - flux_{out}} \tag{28}$$

The error in the mass balance computation is then given by:

$$error_{MBR_m} = 1 - MBR_m \tag{29}$$

which is an indicator of the algorithm efficiency. We used the root mean square error (RMSE) and the percentage relative error (PRE) (the difference between the measured and the estimated value divided by the measured value multiplied by 100) for model verification. The PRE is calculated for every experimental and simulated data pair.

3.2. Model performance assessment

Model performance was assessed by comparing the model output to field measurements of distributed soil water content, distributed perched water depth and integrated streamflow. The root mean square error (RMSE), the R^2 and the Nash–Sutcliffe model efficiency coefficient [42] were calculated for model testing. The Nash–Sutcliffe model is given by:

$$NS = 1 - \frac{\sum_t^T (q_o^t - q_m^t)^2}{\sum_t^T (q_o^t - q_{ave}^t)^2} \tag{30}$$

where q_0 is observed runoff, q_m is modelled runoff, q_{ave} is the average of observed runoff, the superscript t is time and T is the total time for the time series. *NS* efficiencies can range from $-\infty$ to 1, when $NS = 1$ there is a perfect match between modelled and observed data. When $NS = 0$ the model predictions are as accurate as the mean of the observed data, whereas for $NS < 0$ the observed mean is a better predictor than the model since the residual variance is greater than the data variance.

The root mean square error (RMSE) expresses the error between model observations and predictions, the R^2 describes how well the simulated values correlated with the observed values, while the Nash–Sutcliffe (*NS*) efficiency parameter is a normalized RMSE, which represents how well the model describes the observed variability relative to the mean observed value for the selected time period. Finally, flow duration curves (FDC) were computed for the surface runoff.

4. Catchment-scale distributed hydrological experiments and modelling

4.1. The Troy catchment

Data from a small catchment in northern Idaho were used to test the model. A detailed description of the site and of the experiments are given in Brooks [9] and Brooks et al. [11]. Fig. 1 shows a map of the catchment and a schematic of the installed instrumentation. The Troy catchment provides a unique data set of integrated and distributed data, which allowed a detailed model testing. Moreover, the Troy catchment is one of the few sites where distributed time series of perched water depths as well as soil water content are available on a fine grid. The following data were available from March 1, 1999 to September 30, 2002:

- A 5 m digital terrain model.
- A digital map of the spatial distribution of soil depth.
- Meteorological measurements such as hourly shortwave radiation, relative humidity, air temperature, wind speed, and precipitation.
- Soil physical properties such as bulk density, texture, soil water retention curves, vertical and lateral hydraulic conductivity.

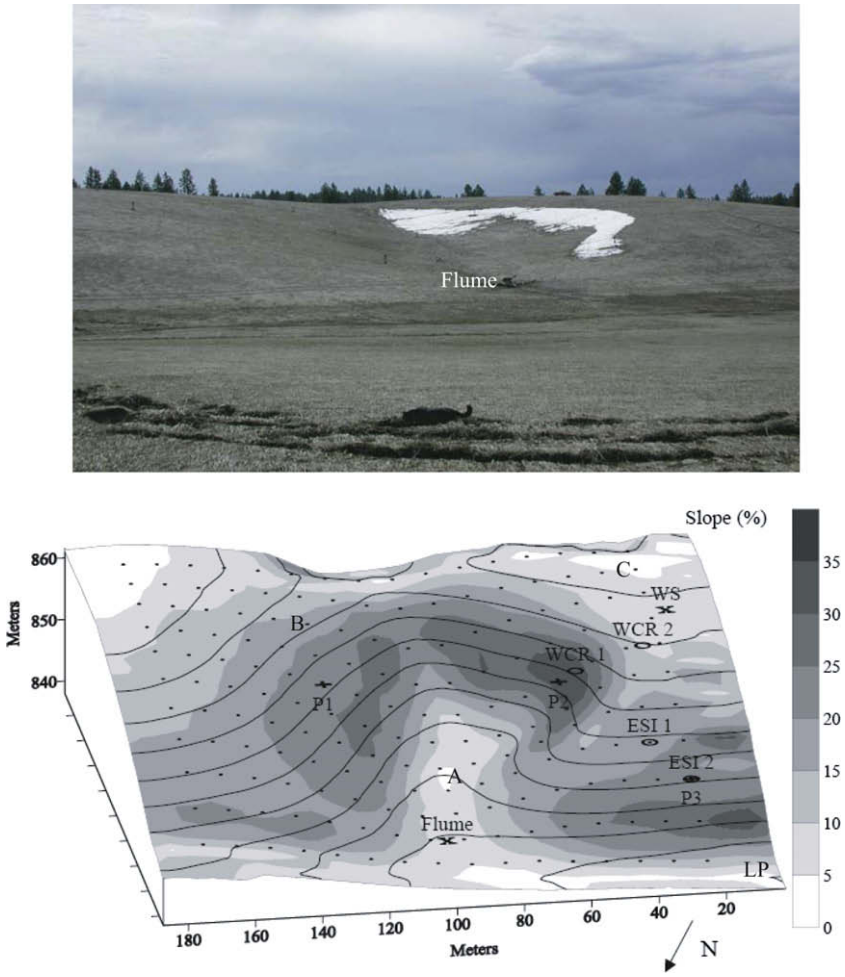

Fig. 1. Picture, map and instrumentation at the Troy catchment. Soil moisture measured with Water Content Sensor (WCR1 and WCR2) are identified with an oval symbol. The location of the weather station (WS) and the surface runoff flume (Flume) are identified with a X symbol. Small dots are locations of shallow wells. Weekly snow water equivalent measurements were made at points (P1, P2, and P3) marked with a + symbol. The wells are indicated by the letters A, B and C. LP is the lowest topographical point. The topography is represented by a 2 m contour map and the shaded land slope in degrees is draped over the figure. (Figure taken from Brooks [9].)

- Perched water level measurements in 176 shallow wells on a 10 m × 15 m grid.
- Three soil water content profiles.
- Snow depths and snow water equivalent.
- Surface runoff measured with a circular flume.

The soils are moderately well-drained with a fragipan (K_s = 0.01–1 cm day^{-1}), high bulk density (ρ_b = 1650 kg m^{-3}), and elevated clay content.

4.2. Model application

4.2.1. Structured grid

The integrated finite difference solution was solved using a structured grid. The horizontal spatial resolution was 5 m, corresponding to the DEM size. The vertical grid was refined, with a finer grid closer to the surface and coarser grid at further depths. In particular, we used a geometrical vertical grid with the following thickness for the first 14 layers (from the soil surface): 2, 2.4, 2.8, 3.5, 4.1, 5, 6, 7.2, 8.6, 10.3, 12.4, 14.9, 17.8, and 20 cm. All the layers below the one of 20 cm thickness, were of equal 20 cm thickness. The model allows for any choice of grid refinement, using either linear of geometric grids at any depth.

4.2.2. Hydraulic properties

Soil water retention curves for the different soil layers were measured by using pressure plates [34], while vertical and lateral saturated hydraulic conductivities were measured as described in Brooks et al. [10]. Basic soil physical and hydraulic properties are

Table 1
Basic soil physical and hydraulic properties for the Troy catchment. (ρ_b bulk density; α, n van Genuchten parameters; θ_r, θ_s residual and saturated water content, K_s saturated hydraulic conductivity.)

Horizon and depth (m)	Sand (%)	Silt (%)	Clay (%)	ρ_b (kg m^{-3})	α (m^{-1})	n (–)	θ_r (m^3 m^{-3})	θ_s (m^3 m^{-3})	K_s (cm day^{-1})
A (0–0.38)	21	70	9	1140	0.57	1.2	0.05	0.58	7.44
B (0.38–0.68)	21	66	13	1130	0.5	1.2	0.05	0.50	2.93
E (0.68–0.86)	21	63	16	1135	0.4	1.1	0.05	0.48	0.96
Fragipan (0.86–2.0)	15	57	28	1650	0.1	1.05	0.07	0.38	0.01

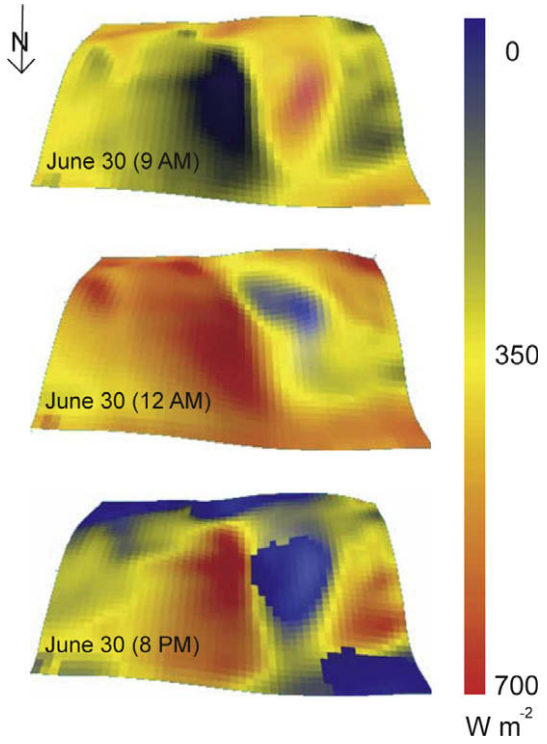

Fig. 2. Computed global solar radiation for the Troy catchment.

listed in Table 1. The vertical K_s listed in Table 1, was obtained by measurements with the Guelph permeameter.

The parameters of the hydraulic functions were obtained by fitting the van Genuchten equation to the experimental water retention data by minimizing the sum of square residuals between experimental data and model, using the Levenberg–Marquardt algorithm [39].

4.2.3. Initial conditions and surface parameters

The initial conditions were of uniform soil water content (at 0.9 degree of saturation) on March 1, 1999. The spring and summer 1999 were used for model spin-up, which is the process of a model adjusting to its initial conditions. Indeed, model's output comparison to experimental data began on October 1999, allowing the model to absorb the initial conditions, for 7 months.

Manning's surface roughness and surface ponding depth were given as a homogeneous parameter over the catchment. The Manning roughness parameter was set at 0.24 s $m^{-1/3}$, which is a common value reported in the literature [45,46]. The thickness of the surface ponding depth can be chosen by the user based on land use and the spatial discretization of the simulation. A thickness of 2 mm was chosen for this study.

4.2.4. The catchment water budget

The model implements an integration of the mass balance, not only at the finite element scale, but also at the catchment scale. This implementation is used for both mass balance tests as well as computation of the water budget at the catchment scale. Therefore, the model output includes a storage term (soil water content), evaporation, transpiration, deep percolation, runoff and subsurface lateral flow, integrated over the whole catchment. The surface runoff and the subsurface lateral flux are computed as fluxes leaving the catchment each hour, at the point LP (lowest topographical point) as indicated in Fig. 1. Soil evaporation, transpiration and deep percolation are computed for each element and integrated over the catchment.

4.2.5. Solar radiation

Fig. 2 shows a map of computed global solar radiation at Troy catchment for June 30, 1999. The different shadows (dark blue) indicate the effect of topography on the incident solar radiation. For instance, on June 30 at 9 AM, the east side of the toe slope was still in shade because of the position of the rising sun on the horizon.

4.2.6. Snow accumulation and snow melt

Fig. 3 shows measured and simulated snow water equivalent at the point P2. The model provided good estimates of snow water equivalent. Both, the melting times and the melting rates, were simulated well. On the other hand, the snow accumulation phases are simulated less accurately. For instance, on January 7, 2002, the model over-predicted the amount of accumulated snow, although on February 9, 2002, the model and the experimental data matched again well. The RMSE's for the locations P1, P2, and P3 over the 3 years were less than 22 mm, which is similar to the results obtained by Brooks [9]. In the Troy catchment, snow melt is one of the dominant hydrological processes, as infiltration, redistribution and surface runoff in springtime is driven by snow melt. At this latitude and complex terrain, it is therefore important to couple hydrological models with robust snow melt algorithms providing topography-dependent solar radiation.

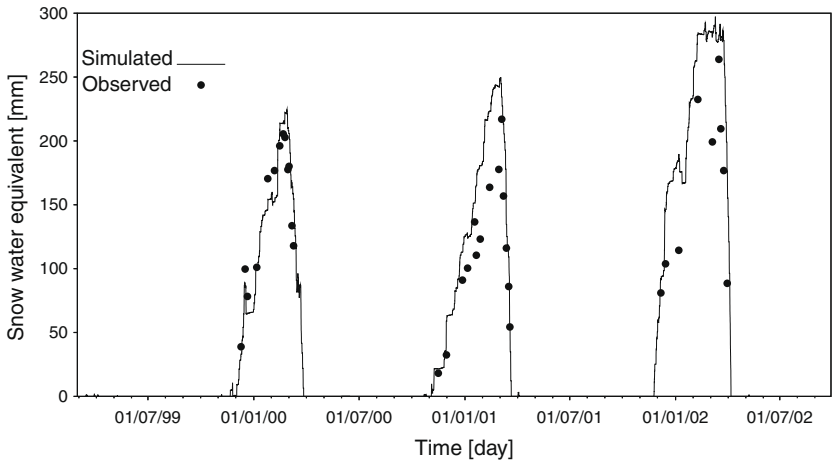

Fig. 3. Observed and simulated snow water equivalent at point P2.

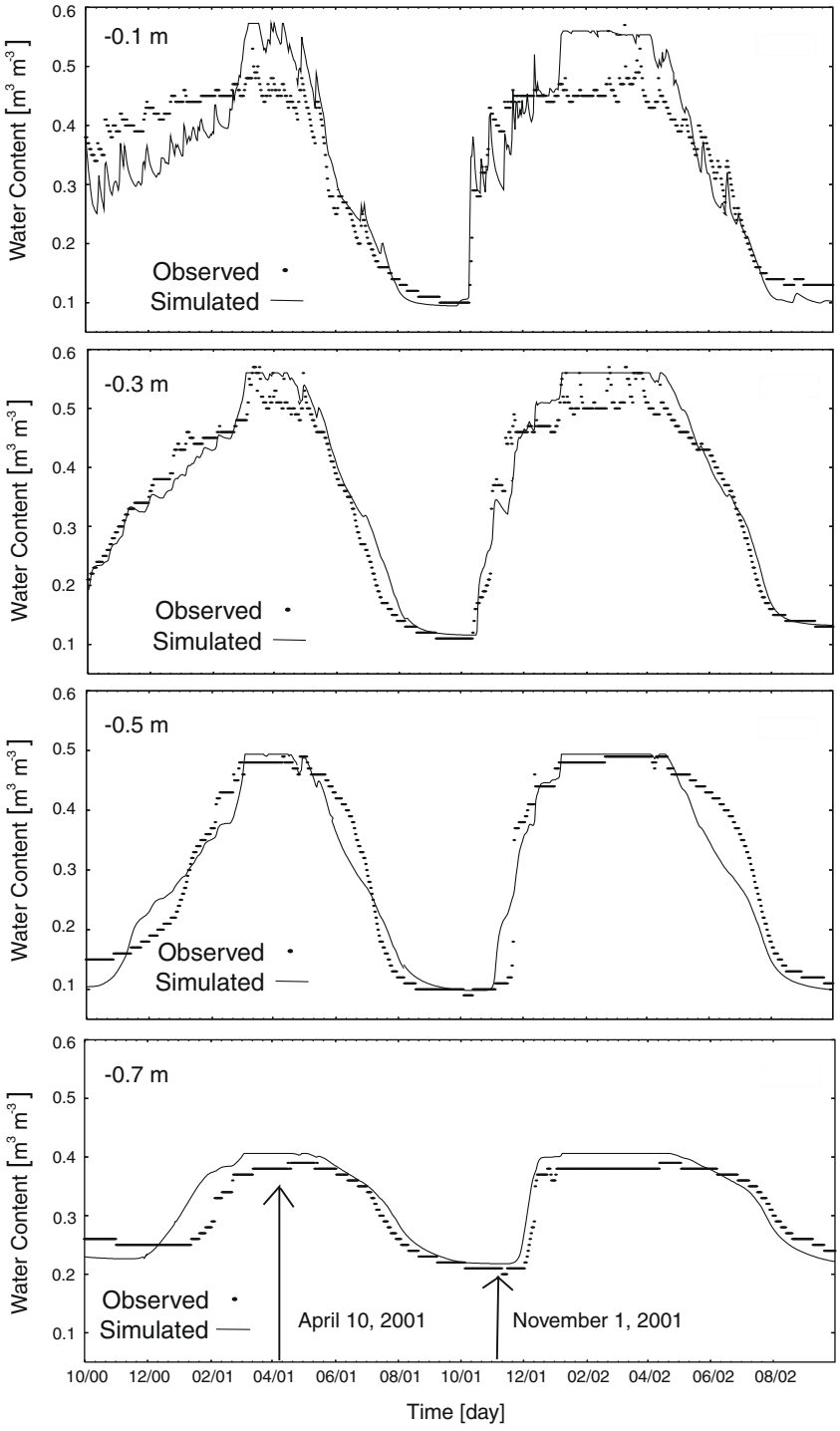

Fig. 4. Experimental (dots) and simulated (lines) daily soil water content at different depths, for the Troy catchment at location WCR1.

4.2.7. Soil water content

Fig. 4 shows the experimental and simulated soil water contents for the Troy catchment. The three-dimensional model allowed to obtain soil water content and soil water potential distributions at each location and time. For comparison, we selected the soil water content output at position WCR1 (Fig. 1), which is in the steeper part of the catchment. The experimental soil water content data were well described by the model with RMSE of 0.0015, 0.0009, 0.001 and 0.0009 $m^3\ m^{-3}$ for the four depths, respectively. An example of a three-dimensional representation of soil water content is shown in Fig. 5. We selected April 1 and November 1, 2001, to show representative soil water contents (shown by the arrows in Fig. 4). On April 10, the topsoil was close to saturation. The high water saturations were due to snow melt (Fig. 3), which provided enough water to wet the profile down to the deepest layer. These results were confirmed by the experimental measurements shown in Fig. 4. The horizontal spatial variation at −0.7 m depth is due to both uneven redistribution due to the topography, and to the variable spatial soil depth distribution for the different horizons.

4.2.8. Perched water depths

A distributed response analysis was performed by testing the model against a large number of perched water depth measure-

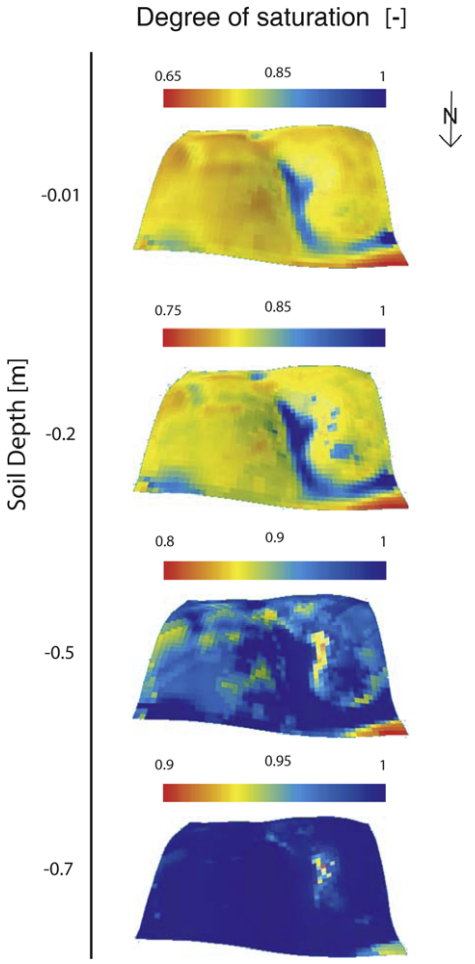

Fig. 5. Water content at the Troy catchment for four different soil depths on April 10, 2001. The simulation was performed on a 5-m grid digital terrain model. The color range is variable for increased visual resolution.

ments. The perched water depths variations are very dynamic because of the presence of a shallow semi-impermeable layer. Brooks et al. [11] reported that the difference between the amount of water held in the soil at saturation and the amount of water in the soil when perching started was only 0.036 m of water, equivalent to a difference in volumetric soil water content of only 5%, between saturation and perching. Therefore, based on the average soil depth, the model must predict the soil water content with a high level of accuracy, corresponding to 1.6% of the true value [9]. The combination of perched water depths and soil water content measurements was a robust combination to test the model performance, and in particular its ability to correctly describe distributed variables. The assessment was performed for seven representative shallow wells, representing different positions within the catchment, and therefore tests the model at different slopes and positions.

Figs. 6 and 7 show the perched water depth fluctuations (well 1,4 and −2,9 in Brooks et al. [11]). The fluctuations were described well, with a Nash–Sutcliffe of 0.41 for the whole experimental period. During the winter 1999–2000, the water table at well A was close to the soil surface. These data were corroborated by the soil water content distribution. During the winter 2000–2001, however, the shallow water table reached the soil surface only in February–March, at the beginning of the snow melt. During the winter 1999–2000 cumulative precipitation in January 2000 was 173 mm, whereas during the winter 2000–2001, cumulative precipitation in January 2001 was only 90 mm. This was due to differences in amount of rainfall and snow, i.e., the snow water equivalent during the winter 2000–2001 was smaller than in 1999–2000 (Fig. 3).

The simulated perched water depth at well B was always higher than the observed perched water depth. Brooks et al. [11] described a discontinuity in the fragipan in this region, where water could percolate through the fragipan. Brooks et al. [11] noted that, because of the high soil moisture retention in these shallow soils, a large error in perched water depth can be caused by a very small error in simulated soil water content.

Fig. 8 shows the perched water depth at well C (well 8,10 in Brooks et al. [11]). This well is located at the catchment divide, being located at the southwest corner of the catchment. The model predictions were close to the experimental measurements. There was an under-estimation of the perched water depth during December and January 2000. As reported by Brooks et al. [11] this is likely due to errors in the estimation of snow melt during this

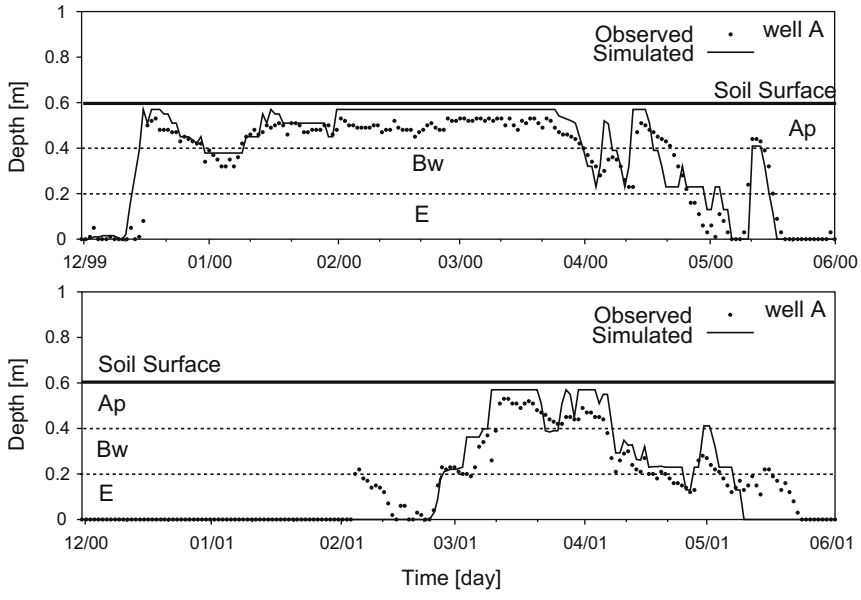

Fig. 6. Simulated and observed perched water depth for the period 2000–2002 at well A.

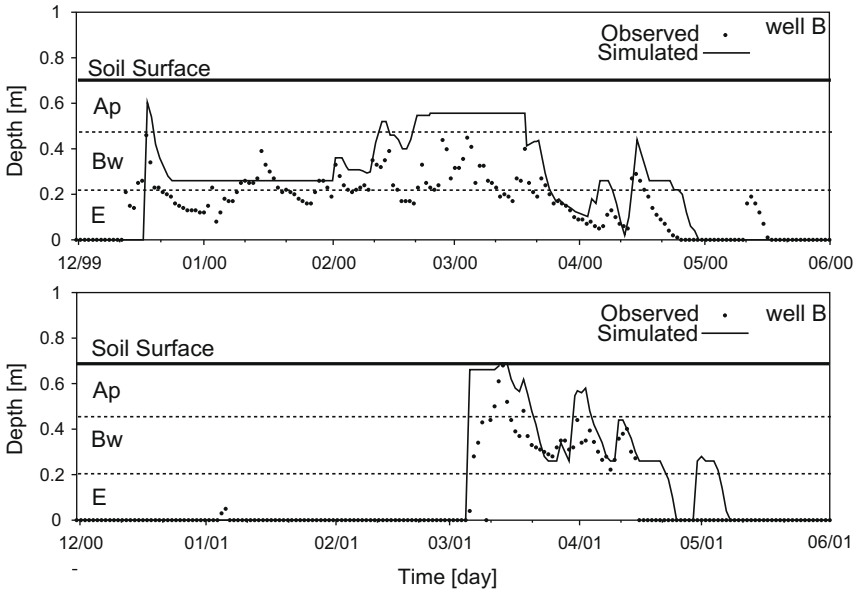

Fig. 7. Simulated and observed perched water depth for the period 2000–2002 at well B.

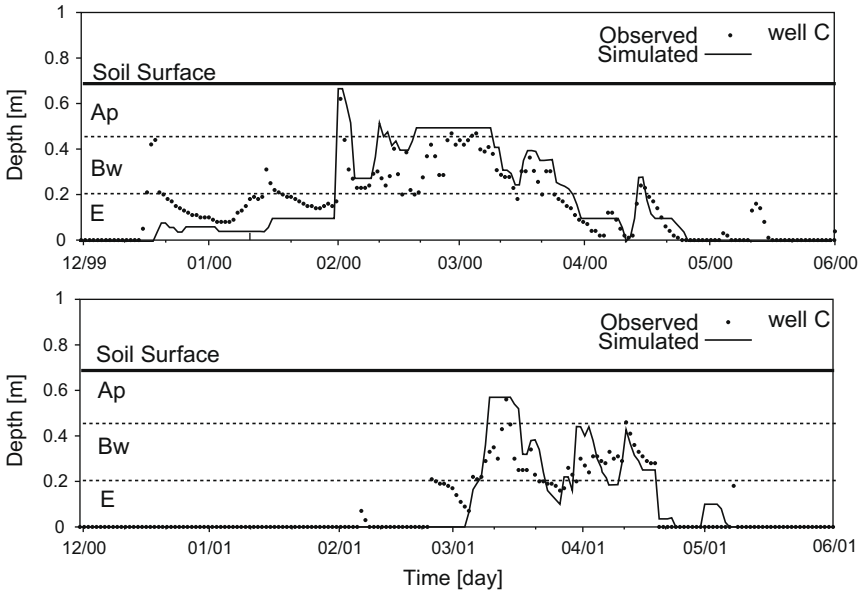

Fig. 8. Simulated and observed perched water depth for the period 2000–2002 at well C.

period, or to experimental errors in the amount of measured precipitation. Precipitation measurements were performed on the site, using an unshielded tipping-bucket rain gauge with an antifreeze siphoning snow adapter during 2001 and 2002. Precipitation data during subfreezing weather for the 2000 winter season were taken from the Moscow, ID, cooperative weather station located roughly 20 km to the west. Differences in local amount of snow, for instance due to snow drifts may have affected the results.

In general, the fragipan was simulated by setting a low value of hydraulic conductivity to simulate the formation of perched water tables. However, fragipans layers are often fractured, with values of conductivity changing in the horizontal direction, and determining variability of vertical water fluxes. Since the horizontal variations of the fragipan conductivity were not measured (they would have required an extensive sampling of the fragipan), we used a uniform value of fragipan conductivity. This is another reason for the discrepancies between the simulated and the measured perched water depths.

4.2.9. Surface runoff

Simulated streamflow were compared with observed discharge at the flume (Fig. 9). In general, the simulation of the streamflow was good (Table 2). Surface runoff simulation was improved in respect to previous simulations with the SMR model [11]. For instance the SMR model yielded a Nash–Sutcliffe parameter for the whole experimental period of 0.29, while Criteria-3D provided a value of 0.39.

We observed that the model-simulated runoff occurred too early in 2001. This can be explained by the behavior of the snow pack itself. Snow accumulation and melt rates changed dramati-

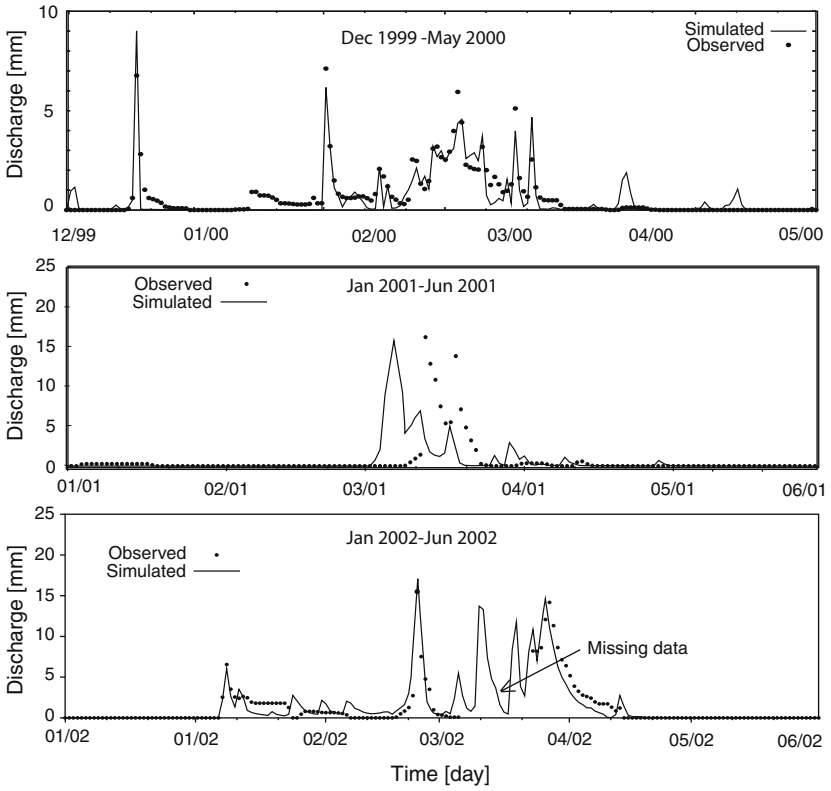

Fig. 9. Predicted and observed hourly discharge for three different time periods.

Table 2
Statistical parameters for the comparison of runoff at the Troy catchment for four different periods.

Time period	RMSE (mm)	R^2	Nash–Sutcliffe
December 1, 1999–May 31, 2000	1.3	0.47	0.45
February 1, 2000–May 31, 2000	2.9	0.15	−1.33
February 1, 2001–May 31, 2001	1.9	0.62	0.65
October 1, 1999–September 30, 2002	1.6	0.63	0.39

cally with spatial position, and snow accumulation was affected by snow drifting. Indeed, the snow pack melted more rapidly on the east side of the catchment, which has more of a southern exposure, than the west side of the catchment. Therefore, the simulated snow water equivalent (which was integrated over the whole catchment) had an influence on the soil water distribution. However, the Criteria model could still not describe the melting dynamics in the spring 2001, even with the topography-dependent solar radiation. Brooks [9] obtained similar results in their simulation, and they suggested that changes in the properties of the snow pack, such as snow albedo and snow pack temperature gradients, are likely the reasons behind the inability of the model to describe this behavior.

In Criteria-3D, topography-dependent solar radiation was included (Fig. 2), and we observed that this component had an important effect on snow melt in the different areas of the catchment. These considerations on the role of snowpack in the generation of runoff, emphasizes this relevant element in hydrological modelling that cannot be neglected in complex terrains. Although, the model performance was good, it was not possible to correctly describe the surface runoff for spring 2001, where snow melt was predicted to occur too early. Brooks [9] observed that during spring 2001, a 10–20 cm layer of water was ponding on the snowpack, with the snowpack acting as a barrier preventing the melted water to leave the watershed. Melting and re-freezing further complicated the snowpack–water interactions. Such mechanisms were not accounted for in the model.

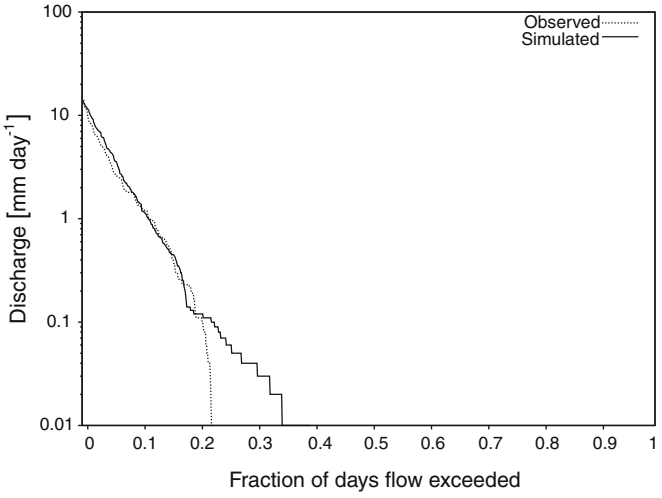

Fig. 10. Flow duration curve for the Troy catchment over a 3-year period.

Finally, we compared the experimental and computed flow duration curves for the entire experimental period (Fig. 10). The flow duration curves are of particular interest insofar as the curves are compared on a logarithmic scale, hence highlighting that the outflow from the catchment is predicted accurately over a large range of values. For the Troy catchment, the flow duration curves indicated that only for fluxes below 0.1 mm day^{-1}, the model could not correctly represent the experimental flow. It can be argued

that, when processes such as water retention in the snow pack play a role determining time shifts in surface runoff, the comparison of flow duration curves is more informative than statistical indexes based on point-wise comparison of values such as Nash–Sutcliffe, R^2, or RMSE.

However, a good agreement between observed and predicted flow duration curves does not necessarily imply a good agreement between observed and predicted water fluxes, and therefore both hydrograph and flow duration curve analysis must be performed to test the model ability to describe the measured fluxes.

4.2.10. Catchment water budget

Computation of the catchment water budget (over the period June 1, 1999–June 1, 2000) provided the following values (in mm): precipitation = 519, runoff = 63, deep percolation = 47, subsurface lateral flux = 18, evaporation = 56, transpiration = 320 and a positive difference in water storage (the soil was wetter on June 2000, than in June 1999) of 15. In terms of total precipitation, the water balance amounted to 12% runoff, 9% deep percolation, 3% subsurface lateral flow, 11% evaporation, 62% transpiration, and a change of water storage of 3%. The low value of lateral subsurface flux was because this variable was computed at a topographical point where the slope was low. However, the dynamic of the soil water content near the flume (in the recharge zone) showed that at steeper slopes, lateral flux was more pronounced. Overall, the catchment experienced long periods when the soil was close to saturation, and runoff was mostly due to snow melt in spring. Although the hydraulic conductivity of the fragipan was low, the prolong periods of soil saturation allowed a considerable amount of deep percolation. The soil water was depleted during the summer and fall seasons by evaporation and transpiration.

5. Conclusions

The Criteria-3D model provided a correct description of the water balance for a small catchment. The model includes all the processes necessary for a complete quantification of the water balance. Spatial patterns of soil moisture proved to be realistic. Important spatially dependent variables such as topography-dependent solar radiation and snow melt are included. These features are desirable when looking for a benchmark assessment in ungauged catchments, and when no data on soil moisture are available. In such cases, distributed models not embedding sufficient physical description often result in aggregated responses which do not allow to identify relevant hydrological mechanisms causing runoff.

A better identification of runoff generating mechanisms is reflected in improved performance statistics. We argue that physically based models are better tools for benchmarking hydrological processes than simpler models. That most of the model input parameters in our study were estimated from physically measured quantities, allows using these types of models in ungauged catchments for the prediction of soil moisture, water table depth, and runoff. However, detailed process-based models are expected to outperform simpler conceptual models to the extent in which catchment's properties are adequately measured and characterized, whereas simple models may be equally accurate when catchment's properties are poorly known.

Acknowledgements

The model was developed through contracts to A. Pistocchi and F. Tomei by ARPA-SIMC, Bologna, in the framework of the Climate Change and Italian Agriculture project (CLIMAGRI), financed by the Italian Ministry for Agricultural, Food and Forestry Policies (Mipaaf), Central Office for Agricultural Ecology (Ucea), and through contracts to F. Tomei and G. Antolini by ARPA-SIMC in the framework of the EU FP6 integrated research project ENSEMBLES, contract number GOCE-CT-2003-505539. A special thank to Vittorio Marletto, Franco Zinoni and Lucio Botarelli for their support, enthusiasm and useful discussions.

Appendix A

A.1. Numerical formulation of the model equations

For subsurface nodes, the nodal mass balance equation (24) can be written as:

$$W_i\left(\frac{d\theta}{dH}\right)_i \frac{\partial H_i}{\partial t} = \sum_{j=1}^{n} \zeta_{ij} K(\theta)_{ij} (H_j - H_i) + q_i \tag{31}$$

where W_i is the soil bulk volume, θ_i is the soil moisture content, K is hydraulic conductivity, H_i is the hydraulic head of node i, and ζ_{ij} is the ratio of bulk exchange area between nodes i and j over the internode distance. The term W_i (as explained in Section 2.2) is used to account for the change in volume of the computational element. Indeed, for the subsurface flow the element volumes are constant and the volumetric water content changes (Richards equation), in the surface flow the element volumes may change as function of the surface hydraulic depth (depending on precipitation, and fluxes in and out from other surface nodes), while the water content of the node is always saturated with water only ($\theta = 1$).

The conductivity dependence on saturation is given by the Mualem [41] and van Genuchten [58] equations, or the modified van Genuchten–Mualem model [31]. The term $(d\theta/dH)_i$ is evaluated through the soil water retention curve as detailed below. For surface nodes, K becomes conveyance, dependent upon water depth (Eq. (6)), ζ_{ij} is the ratio of exchange area between nodes i and j, and the term $W_i(d\theta/dH)_i$ is replaced by the extension of the topographic surface assigned to each surface node. The exchange area between nodes i and j is the product of average water depth in nodes i and j, times the internodal exchange length (which is equal to the grid cell size for regular square grids connected off-diagonals).

Eq. (31) can be written for each of the n nodes (here n is used for number of nodes) of the discretization domain, leading to a system of equations in the form:

$$C\frac{\partial H}{\partial t} = AH + q \tag{32}$$

where C is the diagonal mass matrix with elements:

$$C_{ii} = W_i\left(\frac{d\theta}{dH}\right)_i \tag{33}$$

for subsurface nodes and $C_{ii} = S_{ii}$ for surface nodes, while A is the symmetrical stiffness matrix [3], of which the elements are:

$$A_{ij} = -\sum_{j=1}^{n} \zeta_{ij} K(H)_{i,j} \quad \text{for } i = j \tag{34}$$

$$A_{ij} = \zeta_{ij} K(H)_{i,j} \quad \text{for } i \neq j \tag{35}$$

Both C and A are strongly dependent on the unknown hydraulic heads with non-linear relationship. The time derivative $\partial H/\partial t$ is replaced by its incremental ratio:

$$\frac{\partial H}{\partial t} = \frac{H^{t+1} - H^t}{\Delta t} \tag{36}$$

where the superscripts denote generic times t and $t+1$, with Δt being the time step. By approximating the right-hand-side of Eq. (32) we obtain:

$$H = aH^{t+1} + (1-a)H^t \tag{37}$$

where a is a weighting factor ranging between 0 (explicit) and 1 (implicit). For the modelling in this paper, we used an implicit scheme.

Eq. (32) is then written as:

$$C\frac{H^{t+1}-H^t}{\Delta t} = A(aH^{t+1} - (1-a)H^t) + q \tag{38}$$

or rearranged to highlight the unknowns:

$$\left(\frac{C}{\Delta t} - aA\right)H^{t+1} = \left((1-a)A + \frac{C}{\Delta t}\right)H^t + q \tag{39}$$

By defining:

$$M = \left(\frac{C}{\Delta t} - aA\right), \quad N = \left((1-a)A + \frac{C}{\Delta t}\right) \tag{40}$$

Eq. (39) reads:

$$MH^{t+1} = NH^t + q \tag{41}$$

Both C and A depend on H, which is approximated by H^t, allowing to solve the linearized system of equations, yielding a first approximate solution $H(0)^{t+1}$. With this solution, A and C can be recalculated and the procedure iterated until a certain tolerance in the variation of the subsequent H^{t+1} is met. The tolerance is then checked against the mass balance error. The linear and non-linear defect, or the infinite norm methods, can be choose as convergence criterion.

A.2. Coupling surface and subsurface flow

The surface flow variables are described in Fig. 11, where h_s represent the surface water, which is distinguished into immobile or pond water, h_{pond}, and mobile water, h'_s, defined as $h'_s = \max(0, (h_s - h_{pond}))$. The depth of the pond water, h_{pond}, is defined by the user as input to the model and it can also be spatially distributed as input map. The surface water, h_s, is computed as an average value within the time step, depending on the boundary condition (i.e., precipitation input).

Moreover, the mass exchanges in the surface nodes require distinguishing the following cases depending on the domain to which each node pair belongs. If nodes i and j are both on the surface, Manning's law applies in the form:

$$Q_{ij} = \frac{\left(h'_{s_i}\right)^{5/3} B_{ij}\left(\frac{H_i - H_j}{L_{ij}}\right)^{0.5}}{M_{ij}} \tag{42}$$

where the node i is the one with the highest hydraulic head, B_{ij} is the width of the interface between nodes i and j, $M_{ij} = (M_i + M_j)/2$is the average internode roughness, L_{ij} is the horizontal distance between the nodes, $(H_i - H_j)/L_{ij}$ is the slope of the hydraulic heads.

For nodes i and j both on the surface, for surface flow the matrix A is modified as follows:

$$A_{ij} = \eta_{ij}K_{i,j} \quad \text{for } i \neq j \tag{43}$$

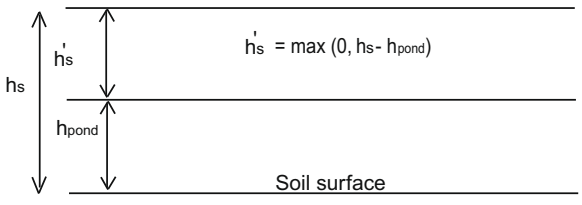

Fig. 11. Schematic describing the surface variables.

with $\eta_{ij} = B_{ij}/M_{ij}(L_{ij})^{0.5}$ and

$$K_{ij} = \frac{\left(h'_{s_i}\right)^{5/3}}{|H_i - H_j|^{0.5}} \quad \text{for } h'_s > 0 \tag{44}$$

otherwise

$$K_{ij} = 0 \tag{45}$$

If nodes i is on the surface and node j is below the surface, a coupled system is determined between surface and subsurface, where the exchange of water is analogous to a one-dimensional variably saturated form of Darcy's law.

Therefore, for nodes i on the surface and node j in the subsurface, the matrix A is modified as follows:

$$A_{ij} = \zeta_{ij}K'_j \quad \text{for } i \neq j \tag{46}$$

where

$$K'_j = \text{mean}(K(H)_j, Ks_j) \tag{47}$$

The main variable is the interface conductivity K'_j which is computed, analogously to the subsurface conductivities, as a geometric or harmonic mean between the conductivity of the first soil node and the saturated conductivity of the interface layer. With this formulation semi-impermeable surfaces (such as roads or sealed soils) can also be considered, by setting very low values of Ks_j. On the other hand, excessive infiltration rates may occur in case of high gradients such as rainfall over a very dry soil. For this case, a limit to the value of K'_j is determined by:

$$K''_j = \min\left(K'_j, \left(\frac{FF_{ij}h_s}{\Delta T}\right)\right) \tag{48}$$

where FF_{ij} is a term (Flux Fraction) that express the fraction of mobile water of node i that can be exchanged with node j. Since the Manning's equation was originally developed for open channel flow, the formulation is written for one dominant direction of flow. When Manning's equation is applied to a complex surface (as for headwater nodes), where more than one flow direction is present, it is necessary to determine a partition of the flow, which is based on the relative slopes (hydraulic head gradients). FF is computed according to the following equation:

$$FF_{ij} = \frac{slope_{ij}}{SumSlopeOut_i} \tag{49}$$

where $slope_{ij}$ is considered positive when $H_i > H_j$ and $SumSlopeOut_i$ is the sum of the slopes between i and the connected nodes with hydraulic head smaller than H_i. This formulation is used to reduce the mass balance error in case of large ΔT and lower numerical accuracy. On the other hand for $\Delta T \to 0$, this limitation becomes negligible.

In general, this formulation allow to use a single continuity equation for both surface and subsurface flow allow to solve Richards' and St. Venant equation simultaneously, without de-coupling of the two processes.

A.3. Computation of the derivatives

The computation of the derivative $\frac{d\theta}{dh}$ (Eq. (2)), which is utilized in the mass matrix C, can be performed at the beginning of the time step, but this value may not represent a correct value for the whole time step, if during the time step there are important variations of the two variables θ and h. In fact, preliminary numerical tests showed that significant over or under-estimation of water fluxes were experienced, depending on the increasing or decreasing behavior of the derivative during the time step. To address this problem, in the code the analytical derivative of the van Genuchten

equation (and of the modified van Genuchten) is computed first at the beginning of the time step, while at the end of each approximation the derivative is computed by the incremental ratio computed on the new values of θ and h obtained at each iteration (Fig. 12). The final value which is used is an intermediate value between the first and the last value. As shown in Fig. 12 by using this approach it is possible to obtain a value of the ratio also in transition between unsaturated and saturated conditions.

The numerical implementation of the model allows the user to choose different numerical methods for solving the system of equations, such as the Gauss–Seidel [40], the over-relaxation [13], or the conjugate gradient [57] methods. In this paper, the system of equation was solved with the Gauss–Seidel method, with a time-step adjusting algorithm, because for this problem the Gauss–Seidel method provided the most precise solution [52]. Since in the Picard iteration scheme the matrix is always symmetric, it can be solved with these different schemes. The numerical solver is implemented in C++. The computation loop scheme is shown in Fig. 13, while the adaptive time step algorithm is described in the next session.

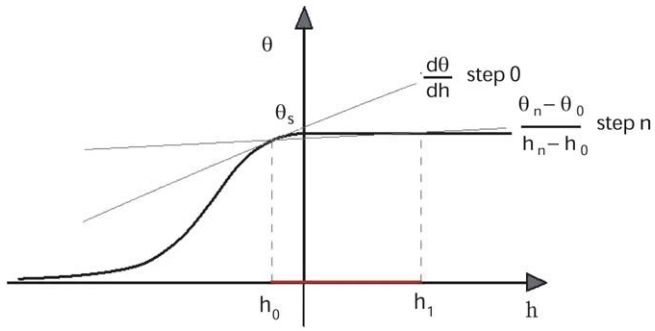

Fig. 12. Example of the calculation of the water capacity. The θ_s indicates the saturated water content and the transition between unsaturated and saturated conditions.

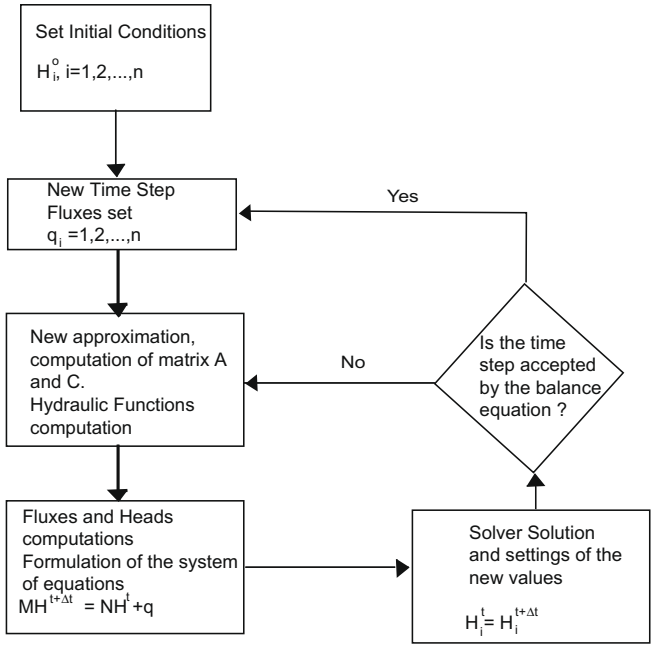

Fig. 13. Flow chart describing the computation loop.

Appendix B

B.1. Adaptive time step algorithm

The model implements a numerical algorithm for adapting the time step, to assure convergence and minimize the mass balance error, but also increased speed when the convergence criteria are easily reached (Fig. 14). For instance, when the pressure head gradients are not steep, convergence is usually easier to achieve and in this case the time step is increased to reduce the computational time. Specifically, at the end of each first approximation, storage and flux are updated based on the reached solution, and the mass balance error is computed based on this first approximation (Eq. (29)). If the error is not below the required tolerance, the algorithm compute a new approximation and check the mass balance error again. If the error is below the tolerance the time step is accepted, otherwise it cut the time step in half and start the computation again. Otherwise if the tolerance in the mass balance error is reached with a low number of approximations, the time step is doubled and the computation is performed again. This adaptive time step algorithm allow therefore to speed up computation when convergence is easily reached (for instance when the water head gradients are not steep and the solution is easily reached). On the other hand when the solution is more difficult to reach (such as in presence of steep water head gradients), the algorithm assure precision by reducing the time step. All the parameters of the algorithm (max time, min time step, tolerance and so forth) are not fixed, but they can be controlled by the user.

Appendix C

C.1. Sensitivity analysis and model tests

A first set of numerical experiments was aimed at determining the correct spatial and temporal discretization steps. It was found that the model was robust in terms of mass balance, which was almost independent of the maximum time step allowed. This is due to the adaptive algorithm which automatically reduces the time step when the mass balance is not within a specified tolerance. The time step, however, must be contained to describe correctly surface flows, and to avoid spurious oscillations in the outflow hydrographs. While the minimum time step seems to have little effect on the simulation, limiting the maximum time step allowed to control oscillations in the initial stage of outflow response. This problem is known in computational hydraulics (see [1]).

A second type of numerical experiments was used to evaluate the discretization convergence properties as suggested by Downer and Odgen [19]. These authors state that vertical discretization in a numerical model of partially saturated soils should be chosen on the basis of the discrepancy in runoff/infiltration/evapotranspiration partitioning of rainfall provoked by coarser and coarser computational cell depths. The authors stress that robustness of spatial discretization steps for the partitioning of rainfall may be strongly dependent on the algorithm chosen to compute hydraulic conductivities at the soil surface. Our numerical tests were referred to the geometry and soil characteristics of the catchment. We performed a series of simulations for various rainfall events and we tested the model response by comparing different spatial discretizations of the vertical profile. Using a top soil layer thickness up to 8 cm had limited effects on the hydrograph shape, but at 12 cm there was significant effect on the hydrograph, indicating that the thickness of the surface layer should not be larger than 8 cm.

A third test was conducted to evaluate the accuracy of the model with reference to the surface water flow component. The test case study was selected from the ones proposed by Di Giammarco

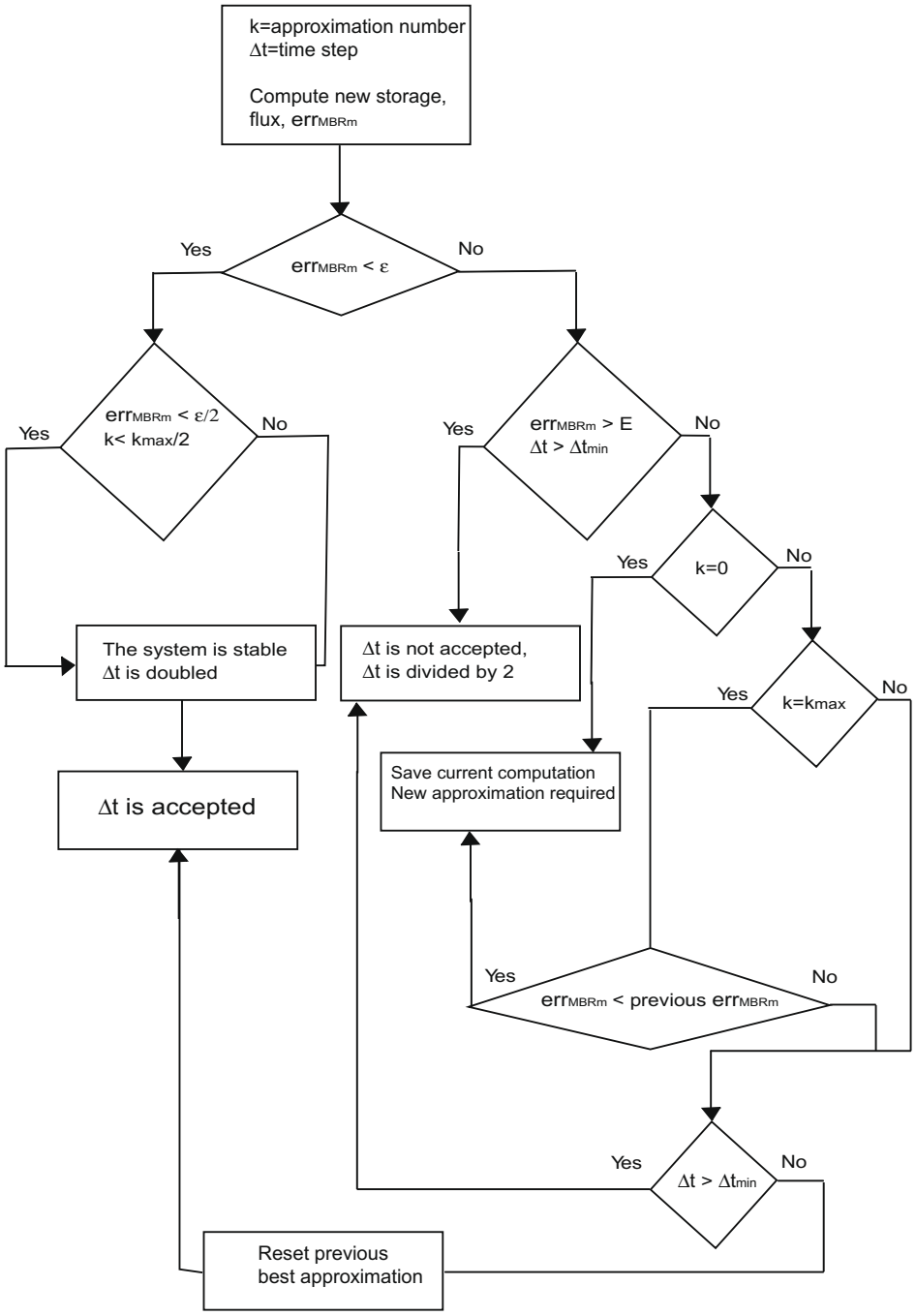

Fig. 14. Flow chart describing the adaptive time step algorithm implemented in the model.

et al. [16] and used by Van der Kwaak [55]. A tilted plane of 800 × 1000 m, with 5% slope was simulated and subjected to a uniform rainfall of 10.8 mm (8640 m^3) for 1.5 h. For such conditions, Di Giammarco et al. [16] presented a comparison of numerical solutions with an analytical solution of the St. Venant's equations under kinematic approximation. Our model produced runoff/discharge consistent with the one reported by Di Giammarco et al. [16], demonstrating the reasonable accuracy of the surface flow component of the Criteria-3D model (Fig. 15). The comparison shown in the figure, was performed for two different values of surface pond (h_{pond}).

Finally, during the model implementation, many additional tests were performed for 1D, 2D and 3D solutions of Richards equation under different initial and boundary conditions. Richards equation was tested: (a) in a laboratory experiment using gamma ray attenuation to measure soil moisture in a soil column, and (b) in a one-dimensional field experiment where Time Domain Reflectometry probes were installed to detect soil water content in a vertical profile. The results of both tests are not shown for brevity, however they both demonstrated the ability of the numerical model to correctly simulate water flow with low errors between experimental and modelled data.

C.2. Model inputs

In general, to be applied in other catchments, the model requires the following input data and parameters:

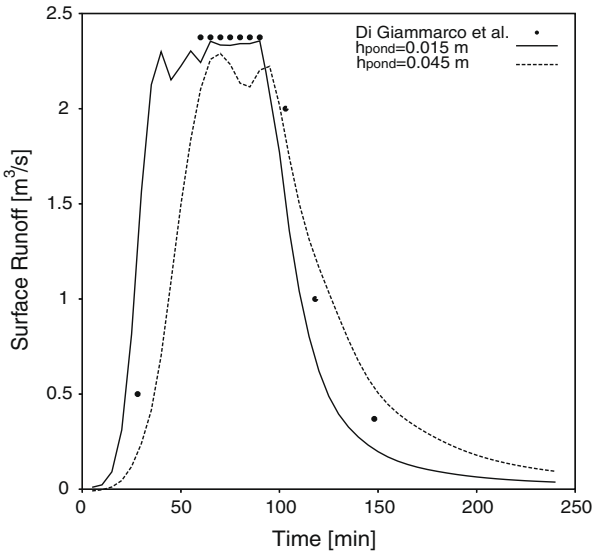

Fig. 15. Numerical experiment for surface runoff. The dots are experimental data from Di Giammarco et al. [16]; the lines are modelled data using the Criteria-3D model, for two different values of the ponding depth parameter.

- A digital elevation map (ESRI floating point format .flt).
- A soil map.
- Meteorological measurements of hourly shortwave radiation, relative humidity, air temperature, wind speed, and precipitation (a weather generator is included in the software for missing weather data).
- Parameters for the hydraulic properties (van Genuchten–Mualem or modified van Genuchten–Mualem models). Pedotransfer functions are included in the software for estimation of hydraulic parameters from simple soil physical variables (texture and bulk density).
- Manning roughness parameter and ponding depth for surface runoff.
- Crop parameters such as LAI, day degrees, root depth and root shape (tables are available for different crops).

References

[1] Abbott M, Refsgaard JC. Distributed hydrological modeling. Heidelberg, Germany: Springer; 1996.
[2] Allen R, Pereira LS, Raes DR, Smith M. Crop evapotranspiration: guidelines for computing crop water requirements. FAO irrigation and drainage paper 56; 1998.
[3] Ames WF. Numerical methods for partial differential equations. 3rd ed. San Diego: Academic Press; 1992.
[4] Arnold JG, Williams JR, Srinivasan R, King KW. Soil and water assessment tool-model description. Technical report Texas Agricultural Experiment Station, USDA-ARS, Grassland, Soil and Water Research Laboratory-Agricultural Research Service Blackland Research Center; 1999.
[5] Bathurst JC, Connell PEO. The system hydrologique Européen. Hydrol Process 1992;6:265–77.
[6] Beven K. Prophecy reality and uncertainty in distributed hydrological modeling. Adv Water Resour 1993;16:41–51.
[7] Beven K, Kirkby MJ. A physically-based variable contributing area model of basin hydrology. Hydrol Sci Bull 1979;24:43–69.
[8] Bristow KL, Campbell GS. An equation for separating daily solar irradiation into direct and diffuse components. Agric For Meteorol 1985;35:123–31.
[9] Brooks ES. Distributed hydrologic modeling of the eastern Palouse. PhD diss., University of Idaho, Moscow, USA; 2003.
[10] Brooks ES, Boll J, McDaniel PA. A hillslope-scale experiments to measure lateral saturated hydraulic conductivity. Water Resour Res 2004;40. doi:10.1029/2003WR002858.
[11] Brooks ES, Boll J, McDaniel PA. Distributed and integrated response of a GIS-based hydrologic model in the eastern Palouse region, Idaho. Hydrol Process 2007;21(611):110–22.
[12] Brutsaert W. Hydrology. An introduction. Cambridge: Cambridge University Press; 2005.
[13] Burden RL, Douglas JF. Numerical analysis. 6th ed. New York: Brooks/Cole Publishing Company; 1997.
[14] Chen ZQ, Govindaraju RS, Kavvas ML. Spatial averaging of unsaturated flow equations under infiltration conditions over areally heterogeneous soils. Water Resour Res 1994;30:523–48.
[15] de Marsily G. Quantitative hydrogeology. San Diego: Academic Press; 1986.
[16] Di Giammarco P, Todini E, Lamberti P. A conservative finite elements approach to overland flow: the control volume finite element formulation. J Hydrol (Amsterdam) 1996;175:267–91.
[17] Doorenbos J, Kassam AH. Yield response to water, 3rd ed., vol. 33. Rome, Italy: FAO Irrigation and Drainage Publication; 1979.
[18] Doten CO, Bowling LC, Lanini JS, Maurer EP, Lettenmaier DP. A spatially distributed model for the dynamic prediction of sediment erosion and transport in mountainous forested watersheds. Water Resour Res 2006;42. doi:10.1029/2004WR003829.
[19] Downer CW, Ogden FL. Appropriate vertical discretization of Richards' equation for two-dimensional watershed scale modeling. Hydrol Process 2004;18:1–22.
[20] Driessen PM, Konijn NT. Land-use systems analysis. Wageningen: Wageningen Agricultural University; 1992.
[21] Flanagan DC, Ascough JC, Nicks AD, Nearing MA, Laflen JM. Overview of the WEPP erosion prediction model. In: Flanagan DC, Nearing MA, editors. USDA water erosion prediction project: hillslope profile and watershed model documentation. West Lafayette, IN: USDA-ARS NSERL; 1995.
[22] Frankenberger JR, Brooks ES, Walter MT, Walter MF, Steenhuis TS. A GIS-based variable source area hydrology model. Hydrol Process 1999;13:805–22.
[23] Gambolati G, Putti M, Paniconi M. Three dimensional model of coupled density dependent flow and miscible salt transport. In: Bear J, editor. Seawater intrusion in coastal aquifers. Dordrecht: Kluwer Acad. Publishers; 1999 [chapter 10].
[24] Gerard-Marchant P, Hively WD, Steenhuis TS. Distributed hydrological modeling of total dissolved phosphorous transport in agricultural landscapes. Part I. Hydrol Earth Syst Sci 2006;10:245–61.
[25] Gottardi G, Venutelli M. A control-volume finite element model for two-dimensional overland flow. Adv Water Resour 1993;16:227–84.
[26] Grayson RB, Blöschl G. Spatial patterns in catchment hydrology: observations and modeling. Cambridge, UK: Cambridge University Press; 2000.
[27] Grayson RB, Moore ID, McMahon TA. Physically based hydrologic modeling. 1. A terrain-based model for investigating purposes. Water Resour Res 1992;28:2639–58.
[28] Haith DA, Shoemaker LL. Generalized watershed loading functions for stream flow nutrients. Water Resour Bull 1987;23:471–8.
[29] Harbaugh AW, Banta ER, Hill MC, McDonald MG. MODFLOW-2000, the US geological survey modular ground water model – user guide to modularization concepts and the ground-water flow process. Open-file report 00-92 Reston, Virginia, USGS; 2000.
[30] Hofierka J, Suri M. The solar radiation model for open source GIS: implementation and applications. In: Proceedings of the open source GIS-GRASS users conference. Trento, Italy: American Chemical Society; 2002.
[31] Ippisch O, Vogel HJ, Bastian P. Validity limits for the van Genuchten–Mualem model and implications for parameter estimation and numerical simulation. Adv Water Resour 2006;29:1780–9.
[32] Ippisch O. Numerik von Trasportprozessen in Porosen Medien. Lecture Notes. Germany: University of Heidelberg; 2009. 256pp..
[33] Jarvis NJ. The MACRO model (version 3.1): technical description and sample simulations. Reports and dissertations, 19, Department of Soil Sciences, Swedish University of Agricultural Sciences; 1994.
[34] Klute A. Water retention: laboratory methods. In: Klute A, editor. Methods of soil analysis. Part 1. Physical and mineralogical methods. Madison, WI: American Society of Agronomy; 1986. p. 635–62.
[35] Linke F. Transmissions koeffizient und trübungsfaktor. Beitr Phys Fr Atmos 1922;10:91–103.
[36] Liston GE, Sturm M. A snow transport model for complex terrain. J Glaciol 1999;44:498–516.
[37] Loague K, Van der Kwaak J. Physics-based hydrologic response simulation: platinum bridge, 1958 Edsel, or useful tool. Hydrol Process 2004;18:2949–56.
[38] Marletto V, Zinoni F, Criscuolo L, Fontana G, Marchesi S, Morgillo A, et al. Evaluation of downscaled DEMETER multi-model ensemble seasonal hindcasts in a northern Italy location by means of a model of wheat growth and soil water balance. Tellus 2005;57:488–97.
[39] Marquardt DW. An algorithm for least-squares estimation of non-linear parameters. J Soc Ind Appl Math 1963;11:431–41.
[40] Morton KW, Mayers DF. Numerical solution of partial differential equations. Cambridge, UK: Cambridge University Press; 1994.
[41] Mualem Y. A new model for predicting the hydraulic conductivity of unsaturated porous media. Water Resour Res 1976;12:513–22.
[42] Nash JE, Sutcliffe JV. River flow forecasting through conceptual models – Part I: A discussion of principles. J Hydrol (Amsterdam) 1970;10:282–90.
[43] Neteler M, Mitasova H. Open source GIS: a GRASS GIS approach. Kluwer Academic Publishers; 2002.
[44] Pan L, Wierenga PJ. Improving numerical modeling of two-dimensional water flow in variably saturated heterogeneous porous media. Soil Sci Soc Am J 1997;61:335–46.
[45] Orlandini S, Rosso R. Parameterization of stream channel geometry in distributed modeling in catchment dynamics. Water Resour Res 1998;34. doi:10.1029/98WR00257.

[46] Orlandini S, Moretti G. Determination of surface flow paths from gridded elevation data. Water Resour Res 2009;45. doi:10.1029/2008WR007099.
[47] Paniconi C, Wood E. A detailed model for simulation of catchment scale subsurface hydrological processes. Water Resour Res 1993;29:1601–20.
[48] Proffitt APB, Rose CW. Soil erosion processes. I. The relative importance of rainfall detachment and runoff entrainment. Aust J Soil Res 1991;29:671–83.
[49] Shaw GJ, Crumpton PI. An assessment of the finite termination property of the defect correction method. Int J Numer Method Fluid 1992;16(3):199–215.
[50] Sivakumar B. Dominant processes concept in hydrology: moving forward. Hydrol Process 2004;18:2349–53.
[51] Svetlitchnyi AA, Plotnitskiy SV, Stepovaya OY. Spatial distribution of soil moisture content within catchments and its modeling on the basis of topographic data. J Hydrol (Amsterdam) 2003;277:50–60.
[52] Tomei F. Numerical analysis of hydrological processes. Master thesis, Faculty of Mathematics, Department of Computer Science, University of Bologna, Italy; 2005.
[53] Troch PA, Paniconi C, van Loon EE. Hillslope-storage Boussinesq model for subsurface flow and variable source areas along complex hillslopes: 1. Formulation and characteristic response. Water Resour Res 2003;39. doi:10.1029/2002WR001728.
[54] Simunek J, Huang K, van Genuchten MT. The HYDRUS code for simulating the one-dimensional movement of water, heat and multiple solutes in variably-saturated media. Research report no. 144, US Salinity Laboratory, Agricultural Research Service, US Department of Agriculture, Riverside; 1998.
[55] Van der Kwaak J. Numerical simulation of flow and chemical transport in integrated surface–subsurface hydrologic systems. PhD diss., University of Waterloo, Waterloo, Ontario; 1999.
[56] Van der Kwaak J, Loague K. Hydrologic-response simulations for the R-5 catchment with a comprehensive physics-based model. Water Resour Res 2001;37:999–1013.
[57] van der Vorst HA. Iterative Krilov methods for large linear systems. Monograph on Applied and Computational Mathematics. Cambridge, UK: Cambridge University Press; 2003.
[58] van Genuchten MT. A closed-form equation for predicting the hydraulic conductivity of unsaturated soils. Soil Sci Soc Am J 1980;44:892–8.
[59] Voss CI, Provost AM. Sutra, a model for saturated–unsaturated variable density ground-water flow with energy or solute transport. US geological survey, Open-file report 02-4231; 2002. 250pp.
[60] Wigmosta MS, Lettenmaier DP. A comparison of simplified methods for routing topographically driven subsurface flow. Water Resour Res 1999;35:255–64.
[61] Wooldridge SA, Kalma JD, Walker JP. Importance of soil moisture measurements for inferring parameters in hydrologic models of low-yielding ephemeral catchments. Environ Model Softw 2003;18:35–48.